International Journal of
Molecular Sciences

MDPI

Article

Inter-Regulation of K_v4.3 and Voltage-Gated Sodium Channels Underlies Predisposition to Cardiac and Neuronal Channelopathies

Jérôme Clatot [1,2,*], Nathalie Neyroud [3,4,5], Robert Cox [1], Charlotte Souil [3,4], Jing Huang [6], Pascale Guicheney [3,4,5] and Charles Antzelevitch [1,7,8]

1 Department of Cardiovascular Research, Lankenau Institute for Medical Research, Wynnewood, PA 19096, USA; CoxR@mlhs.org (R.C.); AntzelevitchC@mlhs.org (C.A.)
2 Division of Neurology, The Children's Hospital of Philadelphia, Abramson Research Center, Room 512C-D, 3615 Civic Center Boulevard, Philadelphia, PA 19104, USA
3 Team "Genomics and Pathophysiology of Myocardial Diseases", Faculté de Médecine Pitié-Salpêtrière, 91 Boulevard de l'Hôpital, Sorbonne Université, UMR_S1166, F-75013 Paris, France; nathalie.neyroud@sorbonne-universite.fr (N.N.); charlotte.souil@gmail.com (C.S.); pascale.guicheney@sorbonne-universite.fr (P.G.)
4 Team "Genomics and Pathophysiology of Myocardial Diseases", Faculté de Médecine Pitié-Salpêtrière, 91 Boulevard de l'Hôpital, INSERM, UMR_S1166, F-75013 Paris, France
5 Institute of Cardiometabolism and Nutrition, ICAN, Pitié-Salpêtrière Hospital, 47-83 Boulevard de l'Hôpital, F-75013 Paris, France
6 Department of Biostatistics, Epidemiology and Informatics, University of Pennsylvania Perelman School of Medicine, Philadelphia, PA 19104, USA; jing14@pennmedicine.upenn.edu
7 Lankenau Heart Institute, Main Line Health System, Wynnewood, PA 19096, USA
8 Sidney Kimmel Medical College, Thomas Jefferson University, Philadelphia, PA 19104, USA
* Correspondence: clatotj@email.chop.edu; Tel.: +1-216-370-2395

Received: 10 June 2020; Accepted: 10 July 2020; Published: 17 July 2020

Abstract: Background: Genetic variants in voltage-gated sodium channels (Na_v) encoded by *SCNXA* genes, responsible for I_{Na}, and K_v4.3 channels encoded by *KCND3*, responsible for the transient outward current (I_{to}), contribute to the manifestation of both Brugada syndrome (BrS) and spinocerebellar ataxia (SCA19/22). We examined the hypothesis that K_v4.3 and Na_v variants regulate each other's function, thus modulating I_{Na}/I_{to} balance in cardiomyocytes and $I_{Na}/I_{(A)}$ balance in neurons. Methods: Bicistronic and other constructs were used to express WT or variant Na_v1.5 and K_v4.3 channels in HEK293 cells. I_{Na} and I_{to} were recorded. Results: *SCN5A* variants associated with BrS reduced I_{Na}, but increased I_{to}. Moreover, BrS and SCA19/22 *KCND3* variants associated with a gain of function of I_{to}, significantly reduced I_{Na}, whereas the SCA19/22 *KCND3* variants associated with a loss of function (LOF) of I_{to} significantly increased I_{Na}. Auxiliary subunits $Na_v\beta$1, MiRP3 and KChIP2 also modulated I_{Na}/I_{to} balance. Co-immunoprecipitation and Duolink studies suggested that the two channels interact within the intracellular compartments and biotinylation showed that LOF *SCN5A* variants can increase K_v4.3 cell-surface expression. Conclusion: Na_v and K_v4.3 channels modulate each other's function via trafficking and gating mechanisms, which have important implications for improved understanding of these allelic cardiac and neuronal syndromes.

Keywords: arrhythmia; Brugada syndrome; spinocerebellar ataxia; Na_v1.5; *SCN5A*; Kv4.3; *KCND3*; *SCN1A*; Na_v1.1; channelopathies

1. Introduction

Variants in *SCN5A*, the gene encoding the cardiac voltage-gated sodium channel, $Na_v1.5$, have been associated with life-threatening arrhythmia syndromes, including Brugada syndrome (BrS). BrS is an inherited cardiac channelopathy associated with a high risk of ventricular tachycardia and fibrillation leading to sudden cardiac death. The typical BrS electrocardiographic (ECG) pattern is characterized by the presence of prominent J waves appearing as ST-segment elevation, usually limited to the right precordial ECG leads, V1-V3 [1]. This ECG phenotype has been attributed to LOF variants in inward currents such as I_{Na} or to gain of function (GOF) variants in outward repolarizing currents such as I_{to} [2,3]. Interestingly, Portero et al. recently reported that expression of $K_v4.3$ can reduce I_{Na} [4]. A fine balance may thus exist between these two currents during the early phases of the action potential (AP). An increase in I_{to} associated with a GOF variants in $K_v4.3$, can simultaneously lead to LOF of I_{Na}. The reduced levels of I_{Na} affects the upstroke (phase 0) and in combination with augmented levels of I_{to} can accentuate phase 1 of the action potential and the phenotypic expression of BrS. $K_v4.3$ is also highly expressed in the brain and contributes to A-type current (I_A) involved in the repolarization phase of the action potential of neurons. I_A regulates subthreshold dendritic excitability and modulates dendritic calcium influx via voltage gated calcium channels in Purkinje cells. $K_v4.3$ LOF variants lead to repolarization defects and reduced cellular excitability, giving rise to spinocerebellar ataxia SCA19/22. Whereas LOF variants in *KCND3* have been linked to SCA19/22, GOF variants have been associated with BrS. Interestingly, some *KCND3* GOF variants (e.g., L450F) have been associated with both BrS and spinocerebellar ataxia SCA19/22 [5]. The reason for this dichotomy is not known and the ionic and cellular basis for SCA19/22 is not well defined. The present study examines the hypothesis that voltage-gated sodium (I_{Na}) and $K_v4.3$ (I_{to}) channels modulate each other's function and that this inter-regulation is mediated by interaction of both α and β subunits forming a megacomplex or channelosome. To do so, we have selected well-characterized genetic variants that have been implicated in Brugada and/or spinocerebellar ataxia SCA19/22 syndromes. The non-conducting mutants R878C, G1743R and E555X of $Na_v1.5$ respectively gating-deficient, trafficking-deficient and missense variant leading to a premature stop codon identified in BrS patients were selected. The GOF Kv4.3-L450F identified in BrS and SCA19/22 and the LOF $K_v4.3$-Δ227F associated with SCA19/22 were selected for study as well. In HEK293 cell line, we examined the effects of genetic variants in *SCN5A* associated with BrS on $K_v4.3$ function by examining the effect of $Na_v1.5$ trafficking-deficient to $Na_v1.5$ trafficking-efficient channels on I_{to} [2,3,6,7]. We then examined the effects of *KCND3* variants associated with BrS and spinocerebellar ataxia SCA19/22, on both $Na_v1.5$ and $Na_v1.1$ function by examining the effect of $K_v4.3$ trafficking-deficient vs trafficking-efficient channels on I_{Na}. Finally, we examined regulation of the I_{Na}/I_{to} balance secondary to expression of the different auxiliary subunits, including: Na_vbeta1, MiRP3 and KCNIP2.

2. Results

2.1. R878C, G1743R and E555X $Na_v1.5$ Variants Affect I_{to}

I_{Na} and I_{to} were recorded from HEK293 cells 36 h after co-transfection with pGFP-*KCND3* and pGFP-*SCN5A*-WT, R878C or G1743R. None of the cells expressing the $Na_v1.5$ variants displayed I_{Na}, (Supplementary Figure S1) consistent with previous reports by us and others showing that R878C and G1743R variants in *SCN5A* abolish I_{Na} [2,8–10]. It is noteworthy that we previously established that E555X mutation leads to expression of non-functioning truncated channels comprised of only the first domain [11]. Interestingly, in the cells expressing variant $Na_v1.5$ channels, peak I_{to} was significantly increased when compared to cells expressing the WT $Na_v1.5$ channel (Figure 1A,B and Table 1). The $Na_v1.5$-R878C gating-deficient but trafficking efficient channel, in addition to abolishing I_{Na} due to major pore dysfunction was associated with the largest increase in I_{to}. These effects are consistent with the conditions known to give rise to the BrS phenotype. Interestingly, the $Na_v1.5$-G1743R trafficking-deficient channel led to a significant 62.9% decrease of peak I_{to}, compared to $Na_v1.5$-WT

due to a −6.2 mV shift of steady-state inactivation (Figure 1A,C and Table 1). Indeed, the −40 mV prepulse used for the I-V curves in Figure 1B, represented by the vertical bar in Figure 1C, led to a greater inactivated fraction of K_V4.3 channels, 67.3% of WT explaining the decrease in I_{to} observed on the I-V curve (Figure 1B and Table 1). I_{to} recovery from inactivation was recorded but no significant difference was noted between WT and any of the *SCN5A* variant channels (Supplementary Figure S2).

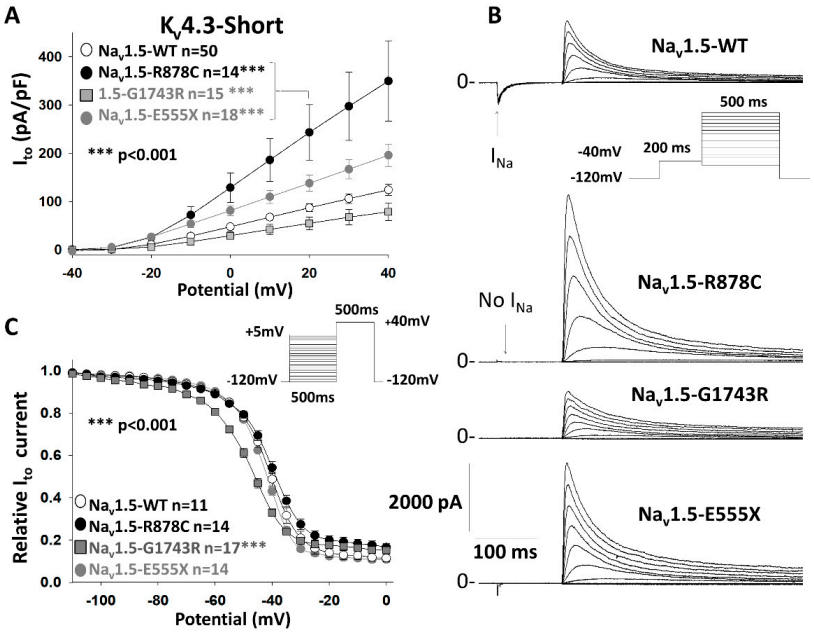

Figure 1. The presence of Na_v1.5 variants affects outward current (I_{to}). (**A**) I_{to} current–voltage relationships recorded from HEK293 cells co-expressing K_v4.3-short (pGFP-IRES-KCND3-Short) channels and either WT, R878C, G1743R, or E555X-Na_v1.5 channels (pcDNA3.1-GFP-SCN5A). (**B**): Representative current traces of I_{Na} in the prepulse followed by I_{to}. Inset shows the voltage protocol employed. The presence of Na_v1.5 variants significantly affect I_{to} compared to WT, at +20 mV, *** $p < 0.001$ for the three variants (In pA/pF; WT = 87.14 ± 8.2, R878C = 243.3 ± 57.55, G1743R = 54.8 ± 12.9, E555X = 138 ± 16.8) (**C**): I_{to} steady-state inactivation. Note: G1743R-Na_v1.5 significantly shifts the steady-state inactivation $V_{1/2}$ of I_{to} compared to WT-Na_v1.5, *** $p < 0.001$. *n* represents the number of recorded cells. In panel A, *n* = 50 WT cells correspond to total of WT cells patched against each variant.

Table 1. Electrophysiological characteristics of Ito in presence of WT and loss of function (LOF) Nav1.5 channels.

Variant	*n*	I_{to} Peak +20 mV	SEM	Fold Change	*p*	*n*	$V_{1/2}$ SSI I_{to}	SEM	Shift	*p*	Relative I_{to}, HP at −40 mV	SEM	Fold Change in Peak I_{to}, HP at −40 mV
WT	50	87.1	8.2	NA	NA	11	−40.03	0.93	NA	NA	48.7	0.03	1
R878C	14	243.3	57.6	2.79	<0.001	14	−39.74	1.2	0.29	NS	54.2	0.03	1.11
E555X	15	138.0	16.8	1.58	<0.001	18	−41.65	0.37	−1.62	NS	43	0.02	0.88
G1743R	18	54.8	12.9	0.63	<0.001	15	−46.22	0.75	−6.19	<0.001	32.9	0.02	0.68

In order to ascertain whether this effect could be due to the short isoform of K_V4.3, another set of experiments was performed using pcDNA3.1-GFP-Na_v1.5 and pGFP-K_v4.3-long isoform (Supplementary Figure S3). The effects observed on peak I_{to} were identical suggesting that these effects are independent of the isoform used.

2.2. LOF and GOF Variants of K_v4.3 Alter I_{Na} from Na_v1.5 and Na_v1.1

In another series of experiments, we sought to determine whether alterations in the expression of K_v4.3 channels can affect I_{Na}. We measured I_{Na} in cells expressing the LOF trafficking-deficient channel Δ227F-K_v4.3, the GOF trafficking efficient L450F-K_v4.3 and WT-K_v4.3. To avoid problems of transfection of multiple plasmids, we engineered a bicistronic construct, p*KCND3-SCN5A*. Thus, we co-transfected the pGFP-*SCN1B* with our WT or variant p*KCND3-SCN5A* bicistronic constructs. The positive green cells displaying the two currents therefore contained all three genes. Interestingly, even in presence of $Na_v\beta1$, the trafficking-deficient K_v4.3-Δ227F significantly increased I_{Na} compared to WT and the GOF K_v4.3-L450F channel led to a significant decrease in I_{Na} when compared to WT and K_v4.3-Δ227F channels (Figure 2A,B; Supplementary Figure S4). Steady-state inactivation of I_{Na} was not significantly affected by the trafficking-efficient or -deficient K_v4.3 channels (Figure 2C). These results strongly support the hypothesis that the ability of K_v4.3 to traffic or not can regulate Na_v1.5 function and likely its trafficking, even in the presence of $Na_v\beta1$. In order to assess whether other voltage-gated sodium channel family members can be similarly affected, we performed experiments in a different model, in which we transfected WT or variant K_v4.3 channels into an HEK293 cell line stably expressing Na_v1.1, $Na_v\beta1$ and $Na_v\beta2$. Very similar results were obtained; I_{Na} was significantly decreased in cells expressing the trafficking efficient K_v4.3-L450F channel and significantly increased in cells expressing the trafficking deficient K_v4.3-Δ227F channel compared to cells expressing the K_v4.3-WT channel. To exclude a potential effect of an overlap between I_{Na} and I_{to}, we designed a protocol allowing us to record I_{Na} free of the influence of I_{to} as explained in the Methods section. Under these conditions, I_{to} remains at the closed state, while I_{Na} recovers by 83.3 ± 0.02% (Supplementary Figure S5). Interestingly, we show that with I_{to} inactivated, I_{Na} recorded from cells expressing K_v4.3-L450F remains significantly reduced compared to those expressing K_v4.3-WT (Supplementary Figure S6). This control experiment excludes a potential overlap between inward and outward current as the cause of the significant decrease of I_{Na} in presence of a larger I_{to}.

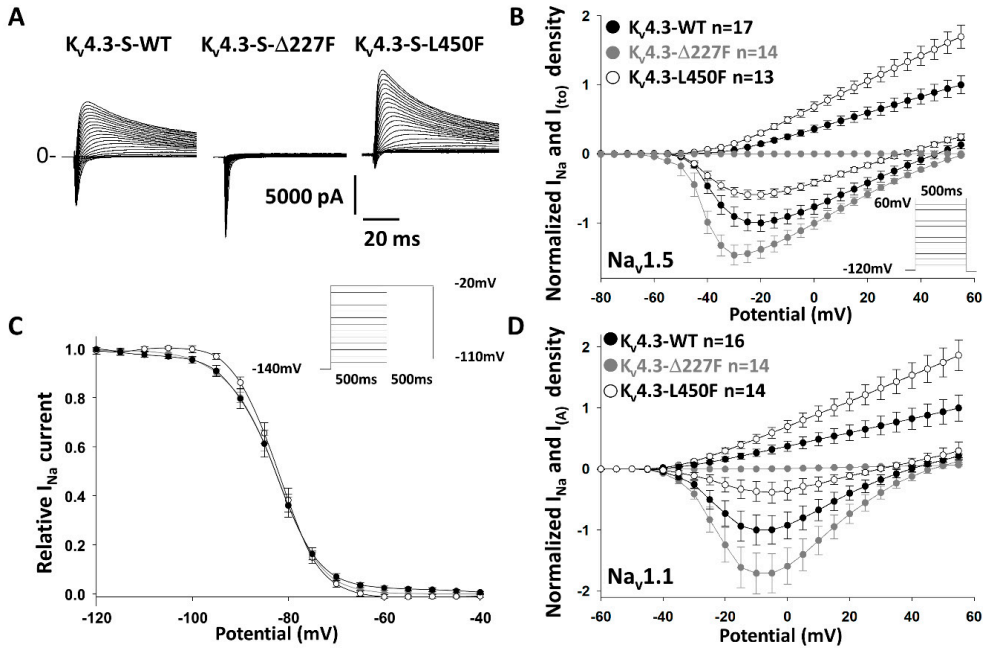

Figure 2. K_V4.3 variants affect I_{Na}. (**A**): Representative traces of I_{to} and I_{Na} measured in HEK293 cells co-expressing the bicistronic construct Na_V1.5/K_v4.3-WT, -Δ227F or -L450F (pKCND3-Short-poliovirus-SCN5A) with $Na_v\beta1$/GFP reporter gene (pGFP-IRES-SCN1B). (**B**): Normalized current–voltage relationships, the trafficking-efficient L450F leads to an increase of I_{to} and a significant decrease in I_{Na} at potentials positive to −35 mV $p = 0.039$ ($p < 0.001$ at −20 mV), whereas

the trafficking-deficient Δ227F-K_v4.3 leads to a decrease of I_{to} but a significant increase in I_{Na} at potentials positive to −45 mV $p = 0.018$ ($p < 0.001$ at −20 mV). (**C**): Steady state inactivation of I_{Na}. K_v4.3 variants did not affect I_{Na} steady-state inactivation. (**D**): Normalized current–voltage relationship in HEK293 cells stably expressing Na_v1.1, $Na_v\beta$1 and $Na_v\beta$2 and transfected with K_v4.3-S WT vs mutants (pGFP-IRES-KCND3-short). The trafficking-efficient L450F leads to an increase of I_{to} but a significant decrease in I_{Na} at potentials positive to −30 mV $p = 0.04$ ($p < 0.001$ at −5 mV), whereas the trafficking-deficient Δ227F-K_v4.3 leads to a decrease of I_{to} but a significant increase in I_{Na} at potentials positive to −20 mV $p = 0.05$ ($p < 0.001$ at −5 mV). Note: *n* represents the number of cells recorded.

2.3. Beta-Subunits of the Megacomplex Regulate the Balance between I_{Na} and I_{to}

To better understand how the interacting proteins of the megacomplex modulate the balance between I_{Na} and I_{to}, we co-expressed the bicistronic construct with several beta-subunits: $Na_v\beta$1 encoded by *SCN1B*, MiRP3 encoded by *KCNE4* or KChIP2 encoded by *KCNIP2*. Co-transfection of *SCN1B* with the bicistronic construct yielded an increase of I_{Na} and a significant decrease in I_{to} (Figure 3A; Supplement Figure S7: Raw traces of Na_v1.5 + K_v4.3 in presence of β-subunits). Co-expression of *MiRP3*, which is known to reduce the trafficking of K_v4.3 channels and therefore I_{to}, significantly increased I_{Na} (Figure 3B; Supplementary Figure S7). Of note, in control experiments, the co-expression of MiRP3 with Na_v1.5 in the absence of K_v4.3, did not modify I_{Na} (Figure 3C), while a drastic reduction of I_{to} was observed in cells expressing only K_v4.3, as expected (Figure 3D).

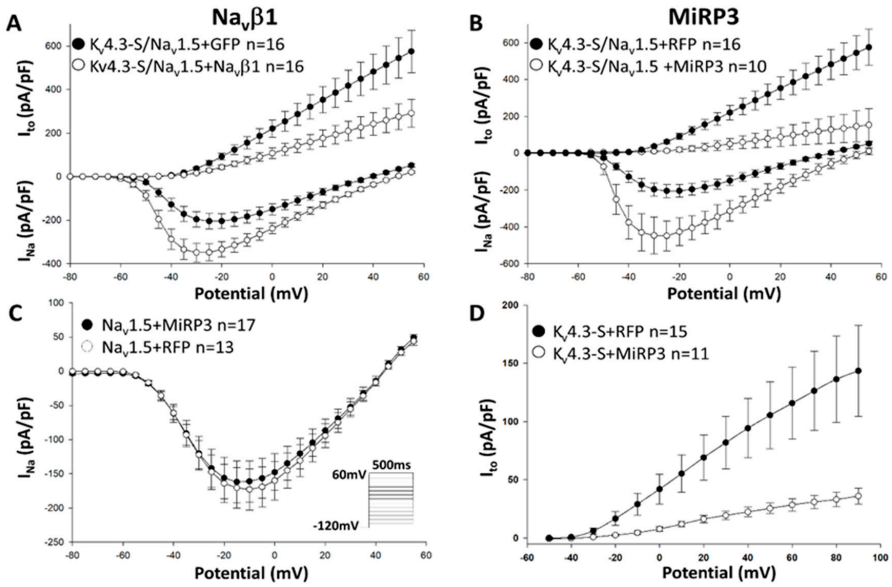

Figure 3. $Na_v\beta$1 and MiRP3 decrease I_{to} and increase I_{Na}. HEK293 cells were transfected with the bicistronic construct Na_v1.5/K_v4.3 (pKCND3-Short-poliovirus-SCN5A), with or without $Na_V\beta$1 (pGFP-IRES-SCN1B vs pGFP) or MiRP3 (pRFP-IRES-KCNE4 vs pRFP) (**A**,**B**), or with Na_v1.5 (pcDNA3.1-GFP-SCN5A)(C), or K_v4.3 (pGFP-IRES-KCND3-Short)(D) with MiRP3. (**A**): Current–voltage relationship measured in HEK293 cells co-expressing the bicistronic construct Na_v1.5/K_v4.3 (pKCND3-Short-poliovirus-SCN5A), with or without $Na_V\beta$1 (pGFP-IRES-SCN1B vs pGFP) showing significant I_{Na} increase in presence of $Na_v\beta$1 at potentials positive to −45 mV $p < 0.001$ ($p < 0.001$ at −20 mV) and I_{to} decrease in presence of $Na_v\beta$1 at potentials positive to −5 mV $p = 0.049$ ($p < 0.001$ at +40 mV) (**B**): I_{Na} increases significantly in presence of MiRP3 at potentials positive to −45 mV $p < 0.001$ ($p < 0.001$ at −40 mV) while I_{to} decreases significantly at potentials positive to −10 mV $p = 0.039$ ($p < 0.001$ at +40 mV). (**C**): In absence of K_v4.3, MiRP3 has no effect on I_{Na}. (**D**): In absence of Na_v1.5, MiRP3 decrease I_{to} at potentials positive to −20 mV $p < 0.001$ ($p < 0.001$ at +40 mV) Note: β-subunits that decrease I_{to} lead to a significant increase of I_{Na} only if both channels, Na_v1.5 and K_v4.3, are present. *n* represents the number of cells recorded.

Similarly, when the bicistronic construct $K_v4.3/Na_v1.5$ was expressed with KChIP2 the expected increase of I_{to} led to a drastic decrease in I_{Na} (Figure 4A; Supplementary Figure S7). In our control experiments co-expression of KChIP2 and $Na_v1.5$, without $K_v4.3$ did not alter I_{Na} (Figure 4B). This result, once again strongly supports that the presence of $K_v4.3$ is required to modulate I_{Na}. In order to ensure that the presence of I_{Na} or I_{to} do not affect each other we calculated the significance of current density of I_{Na} at −40 mV (I_{to}~0) along with I_{to} at +45 mV (closest to I_{Na} reversal potential, I_{Na}~0). Surprisingly, we found that the beta-subunits, MiRP3 and $Na_v\beta1$, which reduce $K_v4.3$ cell surface expression, increased I_{Na}. Moreover, KChIP2, which is known to increase $K_v4.3$ cell surface expression, drastically reduced I_{Na} (Figure 4A); Supplementary Figure S7). These findings provide compelling evidence in support of the hypothesis that changes in I_{Na} are mediated by the presence of $K_v4.3$ channels.

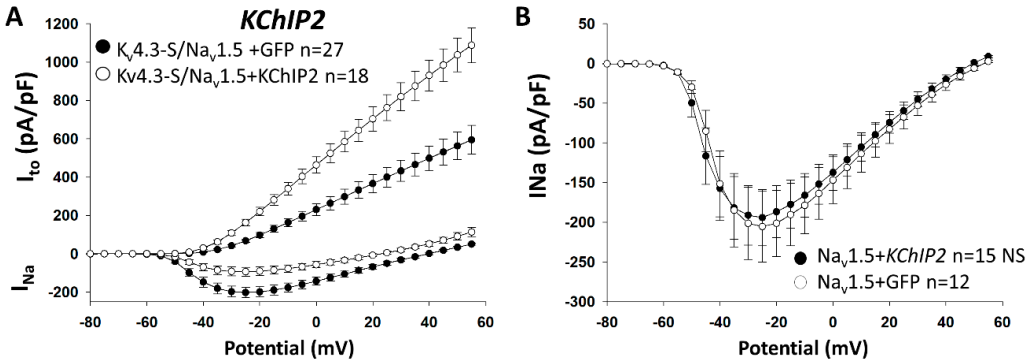

Figure 4. KChIP2 known to increase I_{to} decrease I_{Na}. HEK293 cells were transfected with either the bicistronic construct $Na_v1.5/K_v4.3$ (pKCND3-Short-poliovirus-SCN5A) (A, C), or with $Na_v1.5$ (pGFP-SCN5A) (B), with or without KChIP2 (pGFP-KCNIP2 vs pGFP), $Na_v\beta1$ (pGFP-IRES-SCN1B vs pGFP), or MiRP3 (pRFP-IRES-KCNE4 vs pRFP). (**A**): Current–voltage relationships show that I_{Na} is significantly decreased in the presence of KChIP2 at potentials positive to −45 mV $p = 0.024$ ($p = 0.002$ at −40 mV), whereas I_{to} is significantly increased at potentials positive to −40 mV $p = 0.009$ ($p < 0.001$ at +45 mV). (**B**): In absence of $K_v4.3$, KChIP2 has no effect on I_{Na}. *n* represents the number of cells recorded.

2.4. $Na_v1.5$ and $K_v4.3$ Are Able to Interact

In order to determine whether the inter-regulation between $Na_v1.5$ and $K_v4.3$ channels could be due to an interaction, we performed co-immunoprecipitation assays after co-transfection with tagged-channels (GFP-$Na_v1.5$ and $K_v4.3$-Flag) in HEK293 cells. A positive signal for co-immunoprecipitation was observed for both $K_v4.3$ and $Na_v1.5$ channels (Figure 5A and Supplementary Figure S8). It is noteworthy that $Na_v1.5$-ΔCter (missing the cytoplasmic end of the protein) and $Na_v1.5$-ΔNter (missing the cytoplasmic N-terminus) still co-immunoprecipitated with $K_v4.3$ (Figure 5A and Supplementary Figure S8). Moreover, no signal was detected when immunoprecipitation was performed using the anti-Flag antibody (specific to $K_v4.3$-Flag) on cell lysates expressing only $Na_v1.5$ channel constructs as a negative control. This indicates that immunoprecipitation of $Na_v1.5$ is conditioned and specific to the presence of $K_v4.3$. Taken together, these assays demonstrate that the two channels are able to interact without involvement of the $Na_v1.5$ N- or C-termini. In order to further investigate a potential interaction in living cells, we performed the Duolink technique enabling the visualization of proteins in close proximity in situ. We observed that cells co-expressing both GFP-$Na_v1.5$ and $K_v4.3$-Flag channels show robust positive red signals (Figure 5B). In contrast, cells co-expressing only GFP and $K_v4.3$-Flag, used as negative controls, did not display any red signal, discounting nonspecific interaction between GFP and the $K_v4.3$ channels. Moreover, this experiment allowed us to visualize that $Na_v1.5$ and $K_v4.3$ reside in close proximity (<40 nm) at the membrane but also within intracellular compartments, supporting the hypothesis suggesting trafficking as one of the potential mechanisms regulating the I_{Na}/I_{to} balance.

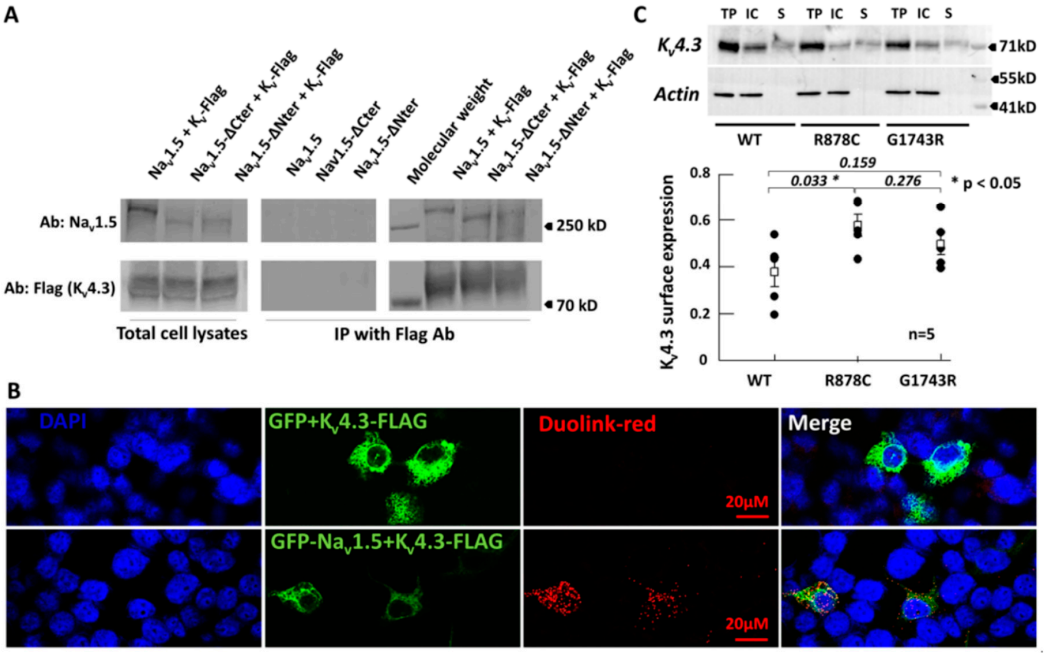

Figure 5. $Na_v1.5$ and $K_v4.3$ interact with each other. (**A**): Co-immunoprecipitation between $Na_v1.5$ and $K_v4.3$. HEK293 cells were transfected with WT or truncated $Na_v1.5$ constructs and $K_v4.3$ (pcDNA3.1-GFP-SCN5A and pCMV-KCND3-Long-Flag) as indicated above the lanes. The total cell lysates were immunoprecipitated with an anti-Flag antibody, specific to $K_v4.3$-Flag, cross-linked to beads. The blots were hybridized with an anti-$Na_v1.5$ antibody (top gels: Blot Ab: $Na_v1.5$) or an anti-Flag antibody (bottom gels: Blot Ab: Flag). The left side corresponds to the total cell lysates of transfected cells before IP. The right side (IP with Flag Ab) corresponds to the elution fractions from beads. The negative control (center of panel A), consisting in an anti-Flag immunoprecipitation in lysates of cells expressing only GFP-$Na_v1.5$ channels, clearly excluded any non-specific interaction between $Na_v1.5$ and $K_v4.3$ channels. The results demonstrated an interaction between $K_v4.3$ and $Na_v1.5$ (n = 7). (**B**): Duolink between GFP-$Na_v1.5$ and $K_v4.3$-Flag. The top line corresponds to cells co-expressing GFP alone (pGFP) with $K_v4.3$-Flag while the bottom line cells co-expressing GFP-$Na_v1.5$ with $K_v4.3$-Flag. Only cells expressing GFP-$Na_v1.5$ and $K_v4.3$-Flag display red positive signals indicating a close proximity between the two channels. Note: Close proximity of the two channels can be observed within intracellular compartments. (**C**)**:** Cell surface biotinylation of $K_v4.3$ in presence of WT, R878C or G1743R GFP-$Na_v1.5$ channels. TP: Total Protein, IC: Intracellular, S: Surface. Note that values of S abundance were not directly quantitated from blots, but calculated as detailed in the method section. The presence of R878C significantly increases the cell surface expression of $K_v4.3$, * p = 0.033 consistent with the observed increase of I_{to}. Note: In cells co-expressing $Na_v1.5$ and $K_v4.3$, the two channels were co-immunoprecipitated.

Additionally, cell surface biotinylation revealed that the $Na_v1.5$-R878C variant enhances cell surface expression of $K_v4.3$ channels (Figure 5C and Supplementary Figure S9), in agreement with our data showing an increase of I_{to} in the presence of the $Na_v1.5$ variant (Figure 1). It is noteworthy that cell surface expression of $K_v4.3$ channels was not significantly different in the presence of the trafficking deficient G1743R-$Na_v1.5$ compared to WT-$Na_v1.5$ (Figure 5B). This result is also in agreement with our electrophysiology recordings showing that the 62.9% loss of peak I_{to} is due to the shift of the steady state inactivation in presence of the −40 mV prepulse. Indeed, in the protocol depicted in Figure 1, a prepulse at −40 mV was used to inactivate the WT sodium channel. This prepulse led to inactivation of a much larger portion of $K_v4.3$ channel in presence of $Na_v1.5$-G1743R compared to $Na_v1.5$-WT, as a result of the steady-state inactivation shift (Figure 1C). Indeed, at −40 mV, 49 ± 0.03% $K_v4.3$ channels are inactivated in presence of G1743R-$Na_v1.5$ compared to WT-$Na_v1.5$ consistent with the loss of function recorded in Figure 1A.

3. Discussion

The voltage-gated sodium channels $Na_v1.5$, responsible for I_{Na}, play a crucial role in excitability and impulse propagation in the heart. $K_v4.3$ channels are responsible for I_{to} which gives rise to phase 1 of the cardiac AP. A fine balance between depolarization and repolarization during the early phase of the AP regulates action potential characteristics. An imbalance between the two currents, in particular a loss of function of I_{Na} and/or a gain of function in $I_{to,}$ can importantly accentuate the AP notch leading to accentuation of the electrocardiographic J wave. Amplification of the J wave often appears as an ST segment elevation in the ECG and can predispose to the development of BrS and/or early repolarization syndrome, which comprise the J-wave syndrome [1,12–15]. $Na_v1.5$ and $K_v4.3$ α-subunits have always been considered to be functionally independent. However, an increasing body of evidence points to the fact that voltage-gated ion channel α-subunits may not function completely independently of each other [2,10,11,16–18].The results described in the present study point to a fundamentally different model of sodium and potassium α-subunits interaction and function. We demonstrate that $Na_v1.5$ and $K_v4.3$ α-subunits interact and inter-regulate each other's function.

Our previous work has shown that voltage-gated sodium α-subunits are able to interact and form functional dimers mediated through recruitment of 14-3-3 proteins regulating the coupled gating of voltage-gated sodium channels responsible for the rapid upstroke of the AP in excitable tissues [2,10,11]. Thus, alteration of trafficking and gating of pathological channels can result in dominant-negative suppression leading to BrS [2,11,19]. We further showed that $Na_v1.1$ and $Na_v1.2$ are able to dimerize, which has far-reaching implications in neurological disorders including epilepsy or spinocerebellar ataxia [10,11,20]. Matamoros, et al. demonstrated that Kir2.1 and $Na_v1.5$ α-subunits interact via α-syntrophin [17]. This interaction modulates the balance between I_{K1} and I_{Na} and supports the concept and importance of exploring the intricacies of megacomplex formation [17]. Their subsequent study demonstrated that Kir2.1 and $Na_v1.5$ share a common pathway of trafficking to the cell surface, thus influencing cell excitability [18]. Consequently, disruption of Kir2.1 trafficking in cardiomyocytes affects trafficking of $Na_v1.5$, which has important implications in the development of arrhythmias associated with inherited cardiac diseases. A recent study also reports interaction [2,11,19] between $K_v4.3$ and $K_v11.1$ (or hERG) proteins, leading to an increase in I_{Kr} current density when $K_v11.1$ and $K_v4.3$ are co-expressed [21]. Finally, Bilicki et al. have shown that a $K_v7.1$ trafficking-deficient variant impairs cell surface expression of $K_v11.1$ by physical interaction of the α-subunits responsible for I_{Kr} and I_{Ks} [22]. The list of auxiliary proteins interacting and regulating the trafficking and the gating of both $Na_v1.5$ and $K_v4.3$ is ever-increasing. $Na_v\beta1$ and SAP97 have previously been identified as important modulators. Recent work from Belau et al., demonstrated that DPP10 a previously known regulator of $K_v4.3$, also regulates the trafficking and gating of $Na_v1.5$ [23]. At last, in support of our hypothesis, Portero et al. recently showed that an increased expression of $K_v4.3$ could lead to a decrease in I_{Na} [4].

In the present study, we investigated the potential for $Na_v1.5$ variants to alter I_{to} and $K_v4.3$ variants to affect I_{Na}. We showed that contrary to traditional belief, $K_v4.3$ and $Na_v1.5$ do not function independently and that they are able to inter-regulate each other, thus modulating their respective trafficking and gating. We were able to show that impairment of $K_v4.3$ trafficking, secondary to expression of *KCNE4*, leads to an increase of I_{Na}. In contrast, increased expression of *KChIP2* produced an increase in I_{to} as well as a decrease in I_{Na}. A representation of this mechanism is schematically represented Figure 6. The J wave or ST segment elevation associated with BrS is known to be more prominent in the right ventricle (RV), accounting for the right ventricular nature of the syndrome. It has long been appreciated that this is due to the presence of a prominent AP notch in right versus left ventricle (LV), which in turn is due to the presence of a more prominent I_{to} in RV versus LV [24]. In support of our hypothesis, a recent study reported that, in addition to a more prominent I_{to}, RV displays a less prominent I_{Na} than LV, thus contributing to the appearance of a more prominent notch and J wave in RV [25].

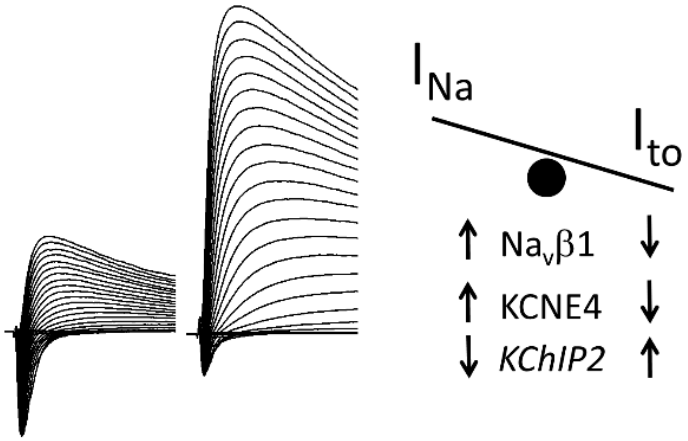

Figure 6. Schematic of the influence of β-subunits of the two channels on the I_{Na}/I_{to} balance. Left panel represents raw traces of I_{Na}/I_{to} displaying a larger I_{Na} and smaller I_{to} as opposed to a smaller I_{Na} and larger I_{to} that could potentially lead to the expression of BrS. The right schematic shows a schematic of the influence of the β-subunits of the two channels on the I_{Na}/I_{to} balance.

Our study shows that *SCN5A* LOF variants can alter I_{to} by modulating $K_v4.3$ cell surface expression (R878C-$Na_v1.5$) or by shifting its steady state inactivation (G1743R-$Na_v1.5$). Reciprocally, the *KCND3* GOF and LOF variants, L450F- and Δ227F-$K_v4.3$, are capable of decreasing and increasing I_{Na} from both $Na_v1.5$ and $Na_v1.1$ channels respectively, strongly suggesting that similar mechanisms of regulation are present in the heart and in the brain. We then sought to investigate whether the nonsense variant E555X could also alter I_{to}. Interestingly, the E555X variant was originally uncovered in a young child with BrS. Park et al. generated a pig model of this variant (E558X) in an attempt to recapitulate the Brugada phenotype in the pig [26]. Unlike in humans, in the pig this mutation led to cardiac conduction defect rather than BrS, with no hint of an ST-segment elevation or J wave in the ECG, even when challenged with the sodium channel blocker flecainide [26]. This was not surprising given that $K_v4.3$ is not expressed in the pig ventricle, which lacks I_{to} [1]. This finding, together with those reported by others [13,27,28] strongly support that the presence of a prominent I_{to} would lead to the expression of BrS/ERS as opposed to only cardiac conduction defect as a consequence of $Na_v1.5$ LOF mutations. The present study provides further evidence in support of this hypothesis, demonstrating a significant increase in I_{to} by this nonsense mutation that causes total loss of I_{Na}. The effect of these genetic variants to produce reciprocal modulation of $K_v4.3$ and $Na_v1.5$ ion channel activity leads to a synergistic shift in the balance of currents in the early phases of the RV epicardial action potential, thus accentuating the J wave or ST segment elevation in the ECG and the BrS phenotype. Inter-regulation of sodium channels with $K_v4.3$ pathogenic variants also provides new insights into factors contributing to potential mechanisms underlying the expression of spinocerebellar ataxia. Autosomal dominant cerebellar ataxias (SCAs) are progressive neurodegenerative disorders resulting from atrophy of the cerebellum leading to progressive ataxia of gait and limbs, as well as speech and eye movement difficulties [29]. Intriguingly, some SCAs and BrS possess striking similarities. They can be both associated with a loss of function of I_{Na} or a gain of function of $K_v4.3$ channels. Indeed, we previously demonstrated a key role for the N-terminus of $Na_v1.5$ in channel trafficking [2], since variants in this region lead to retention of the variant in the endoplasmic reticulum and to BrS [2]. Likewise, Sharkey et al. reported a similar trafficking defect for $Na_v1.6$ (*SCN8A*) N-terminal variants associated with ataxia [30]. These authors demonstrated that the channel is retained in the cis-Golgi resulting in reduced levels of $Na_v1.6$ at the nodes of Ranvier in vivo. To date, 22 causal genes have been associated with spinocerebellar ataxia [29,31]. Twelve variants in *KCND3* have been associated with spinocerebellar ataxia (SCA19/22). Ten of these variants have been shown to cause a LOF and two a GOF of I_A [5,7,32–37]. However, the mechanism whereby $K_v4.3$ GOF mutation lead to SCA19/22 remain ununderstood. Interestingly,

the two GOF variants, p.L450F and p.G600R located in the C-terminus of the channel have also been previously reported to be associated with BrS. Moreover, a missense variant in the C-terminus, p.R431C, was linked to episodic ataxia [38] and a de novo duplication of *KCND3* was reported to cause early repolarization syndrome [39]. Furthermore, Takayama et al. recently reported the $K_v4.3$ GOF variant, p.G306A, to be responsible for early repolarization syndrome, refractory epilepsy, intellectual disability and paroxysmal atrial fibrillation [40]. Collectively, these studies provide further support for the hypothesis that GOF variants in *KCND3* may share a common pathway to cardiac and neuronal channelopathies sometimes in the same patient.

The L450F variant of *KCND3* studied in the present study has been associated with both BrS and SCA19/22 [3,41]. The L450F-$K_v4.3$ mediated GOF in I_{to} in the heart is consistent with the ionic mechanisms causing BrS. Although a similar GOF in $I_{(A)}$ was reported to cause spinocerebellar ataxia SCA19/22, the specific disease mechanism remains to be fully elucidated. Our findings suggest that the $K_v4.3$ GOF variants may give rise to ataxia due to a significant decrease of I_{Na} rather than an increase of $I_{(A)}$ [5]. This hypothesis remains to be more fully tested.

Until recently, studies of *SCN5A* or *KCND3* variants have generally been approached with the traditional view that they are likely to exert an influence on I_{Na} or I_{to}, exclusively. Our findings highlight the need to expand our view of the megacomplex, also termed "the channelosome" to include association of $Na_v1.5$ and $K_v4.3$ α-subunits regulating each other's trafficking and gating. It is not yet known whether interaction between $Na_v1.5$ and other potassium channels such as Kir2.X and $K_v4.3$ occurs in the same mega-complex and how their interaction impacts the dimerization of sodium channels. We could speculate that interactions between different α-subunits could also regulate the subcellular location of the channelosome, e.g., intercalated discs *vs* lateral membrane in cardiac myocytes or axon *vs* initial segment in neurons. Indeed, it was shown that distinct pools of $Na_v1.5$ channels are directed either toward the lateral membrane as opposed to intercalated discs depending on whether they interact with α-syntrophin or SAP97 [42–44]. Our observations provide new insights into a wide range of cardiac and non-cardiac channelopathies, including epilepsy and spinocerebellar ataxia. The resulting paradigm shift is likely to open new perspectives for genetic screening of cardiac arrhythmia and other channelopathies caused by *SCNXA* or *KCND3* variants. The knowledge gained may also be helpful in the design of novel approaches to therapy for these allelic syndromes.

4. Methods

4.1. cDNA Cloning and Mutagenesis

The following plasmids, all containing human channel subunit sequences, were used in this study: pcDNA3.1-GFP-SCN5A [2], pcDNA3.1-GFP-SCN5A-L1821fsX10 (= ΔCter), pGFP-N3-SCN5A-ΔNter generated by truncation of the 381 first nucleotides of SCN5A (127 amino acids), and replacement of residue 128 by a methionine (= ΔNter) [2], pGFP-poliovirus-SCN5A [11], pGFP-IRES-KCND3-Short and pCMV-KCND3-Long-FLAG. The bicistronic construct pKCND3-short-poliovirus-SCN5A plasmid was performed by Genscript (Piscataway, NJ, USA), SCN5A and KCND3 genes were subcloned and inserted into the pGFP-IRES plasmid by substituting GFP by KCND3-short. The pGFP-IRES-SCN1B, pDS-RED-IRES-KCNE4, pDS-RED-IRES, pGFP-IRES-KCNIP2 and pGFP-IRES were used to study the effect of the beta subunits with the bicistronic plasmid. Their coding sequences were CCDS844.1 for the-short isoform of *KCND3* and CCDS843.1 for the long, CCDS 2456.2 for *KCNE4,* CCDS41562.1 for *KCNIP2,* and CCDS 46047.1 for *SCN1B.* Variants were prepared using the QuikChange II XL Site-Directed Mutagenesis Kit (Agilent Technologies/Stratagene, Santa Clara, CA, USA) according to the manufacturer's instructions and verified by sequencing.

4.2. HEK293 Cell Culture and Transfection

HEK293 cells were maintained in DMEM supplemented with 10% heat-inactivated fetal calf serum and 1% penicillin/streptomycin. For patch-clamp recordings, transfections were done with Polyfect transfection (Qiagen, Germantown, MD, USA) according to the manufacturer's instructions and cells were transfected with the constructs of interest in 35-mm well dish, with a total of 0.6 μg of pCDNA3.1-GFP-*SCN5A* and 0.3 μg of *KCND3* construct, molar ratio 2 to 1. Experiments using the bicistronic construct used 1.0 μg of bicistronic construct and 0.5 μg of the Beta IRES GFP subunit of interest in a ratio 2 to 1, per 35 mm dish. HEK293 $Na_v1.1$, $Na_v\beta1$, $Na_v\beta2$ stable cell lines were a generous gift of Dr. Alfred George, Jr. from Northwestern University, Chicago, IL.

For co-immunoprecipitation experiments, cells were transfected with 1.5 μg of each channel plasmid per 25-cm^2-culture flask using jetPEI (Polyplus Transfection, New York, NY, USA), except for negative controls using cells expressing only $Na_v1.5$ constructs. All experimental data provided were performed with a minimum of 3 independent transfections; the *n* in electrophysiology figures represents the number of cells recorded.

4.3. Solutions for Electrophysiological Recordings

Thirty-six hours after transfection, HEK293 cells were trypsinized and seeded to a density that enabled single cells to be identified. Green positive cells were chosen for patch-clamp experiments. For patch clamp recordings, cells were bathed in an extracellular Tyrode's solution containing in mM: 150 NaCl, 2 KCl, 1 $MgCl_2$, 1.5 $CaCl_2$, 1 NaH_2PO_4, 10 glucose, 10 HEPES, pH 7.4 (NaOH). Patch pipette medium was in mM: 125 KCl, 25 KOH, 1 $CaCl_2$, 2 $MgCl_2$, 4 K-ATP, 10 EGTA, 10 HEPES, adjusted to pH 7.2 with KOH. For I_{Na} recording only in Supplemental Data Figure S1, cells were bathed in an extracellular Tyrode solution containing in mM: 135 NaCl, 4 KCL, 2 $MgCl_2$, 2.5 $CaCl_2$, 1 NaH_2PO_4, 20 glucose, 10 HEPES, adjusted to pH 7.4 with NaOH. Patch pipette medium was in mM: 5 NaCl, 140 CsCl, 2 $MgCl_2$, 4 Mg-ATP, 5 EGTA, 10 HEPES, adjusted to pH 4.2 with CsOH. For recording of I_{to} in Figure 3D, extracellular was in mM: 140 NaCl, 4 mM KCl, 2 $CaCl_2$, 1 $MgCl_2$, 5 HEPES, 10 Glucose, adjusted to pH 7.4 with NaOH. Intracellular solution was in mM: 125 KCl, 25 KOH, 1 $CaCl_2$, 2 $MgCl_2$, 4 K-ATP, 10 EGTA, 10 HEPES, adjusted to pH 7.2 with KOH.

4.4. Electrophysiological Recordings

Patch-clamp recordings were carried out in the whole-cell configuration at room temperature. Ionic currents were recorded with Axopatch 200B (Axon Instruments, San Jose, CA, USA) amplifier. Patch pipettes (Corning Kovar Sealing code 7052, WPI, Sarasota, FL, USA) had resistances of 1.2–2.5 MΩ in the whole cell configuration. Voltage errors were reduced via series resistance compensation below 5 mV. Currents were filtered at 5 kHz (−3 dB, 8-pole low-pass Bessel filter) and digitized at 30 kHz (NI PCI-6251, National Instruments, Austin, TX, USA). Data were acquired with pClamp 10 and analyzed with Clampfit (Axon Instruments, San Jose, CA, USA).

To measure peak I_{Na} or I_{to} amplitude and determine current-voltage relationships (I-V curves), currents were elicited by 500 ms-test potentials from −100 to +60 mV by increments of 5 mV from a holding potential of −120 mV. To record I_{Na} free of the influence of I_{to}, we inactivated I_{to} by introducing a 500 ms prepulse at 0 mV, which activates both channels. The test was introduced following a 10 ms inter-pulse interval at −120 mV. Because I_{Na} but not I_{to} recovers from inactivation during the 10 ms interval, I_{Na} can thus be recorded in the absence of I_{to} (Supplement Data Figure S6). For determination of steady-state inactivation of $I_{Na,}$ a holding potential of −120 mV was used and a 500 ms conditioning prepulse was applied in 5 mV increments between −140 and −30 mV, followed by a 500-ms test pulse at −20 mV. For I_{to} steady-state inactivation the conditioning prepulses were performed between −120 mV and 0 mV, followed by a 500-ms test pulse at 40 mV.

Data for the activation-V_m and steady-state availability-V_m relationships of I_{Na} were fitted to the Boltzmann equation as described in Clatot et al. [11].

4.5. Co-Immunoprecipitation

Forty-eight hours after transfection with channel constructs, HEK293 cells were washed with phosphate buffer saline (PBS) and whole cell protein lysates were isolated using lysis buffer (50 mM Tris pH 7.5, 150 mM NaCl, 2 mM EDTA, 1% Triton and protease inhibitor cocktail from Sigma-Aldrich, Saint Louis, MO, USA). Cell pellets were flushed 20 times through a 25-gauge needle, rotated for 1 h at 4 °C, and finally centrifuged for 30 min at 16,000× *g*. Dynabeads Protein G (Invitrogen, Waltham, MA, USA) washed twice with PBS-tween 0.02%, were, either used to pre-clear total proteins for 1 h at room temperature, or incubated with the anti-Flag antibody (Sigma-Aldrich, Saint Louis, MO, USA) for 2 h at room temperature, washed twice again with PBS-tween 0.02%, and incubated with the pre-cleared lysates. Samples were rotated overnight at 4 °C. After washing the beads 4 times with PBS-tween 0.02%, proteins were eluted with the Laemmli sample buffer at 37 °C for 30 min under agitation, separated on a NuPAGE 7% Tris-Acetate gel (Invitrogen), transferred to a nitrocellulose membrane and incubated with primary antibodies: mouse anti-Flag (1:500, Sigma-Aldrich), rabbit anti-$Na_v1.5$ antibody (1:200, Alomone Labs, Jerusalem, Israel), and mouse anti-transferrin receptor (1:500, Invitrogen) as a loading control. Bound antibodies were detected using DyLight-conjugated secondary antibodies (Thermo-Fisher, Waltham, MA, USA), and protein signals were visualized using a Li-Cor Odyssey (Li-Cor Biosciences, Lincoln, NE, USA).

4.6. Duolink

The Duolink technique enables the detection and visualization of protein interactions in tissue and cell samples prepared for microscopy. Duolink detection was performed on HEK293 cell cultures fixed with methanol for 5 min at −20 °C. Cells were then washed twice for 5 min with PBS, blocked in PBS-5% BSA for 30 min at room temperature. Cells were incubated for 1 h with primary antibodies: rabbit anti-GFP (1:300, Torrey Pines Biolabs, Houston, TX, USA) against $Na_v1.5$-GFP or GFP, mouse anti-Flag (1:300, Stratagene) against $K_v4.3$-Flag. The pair of oligonucleotide labeled secondary antibodies (PLA probes from Millipore Sigma, Burlington, MA, USA) was used following manufacturer's instructions and imaging was performed using confocal microscope.

4.7. Cell Surface Biotinylation

Surface proteins of cells on 35-mm dishes were biotinylated using a cross-linking reagent (EZ-Link Sulfo-NHS-S-S-Biotin, Pierce Biotechnology, Rockford, IL, USA). HEK293 Cells were washed three times with ice-cold PBS-CM (PBS + 1 mM $MgCl_2$ and 0.1 mM CaCl2), and 1 mg/mL of biotinylation reagent in 2.5 mL of biotinylation buffer (BB in mM: 150 NaCl, 2 CaCl2, and 10 triethanolamine) or buffer alone was added for 30 min on ice. After the cells were washed with quenching buffer (PBS-CM + 192 mM glycine and 25 mM Tris at pH7.5), whole cell protein lysates were isolated using Triton lysis buffer (in mM: 150 NaCl, 1.5 MgCl2, 20 HEPES, 1% Triton X-100, and 10% glycerol, pH 7.5) with protease and phosphatase inhibitors. Biotinylated proteins were recovered from the cell lysates with prewashed streptavidin-coated agarose beads (Sigma Chemical, Rockford, IL, USA). Proteins in the biotinylated (S = cell surface) and non-biotinylated (IC = intracellular fraction) fractions along with total lysates (TL) were separated by Western blot, transferred to PVDF membranes then probed with anti-Flag (1:1000) followed by anti-actin (1:1000) antibodies. Luminescence (Clarity, BioRad, Hercules, CA, USA) was detected using a ChemiDoc scanner (BioRad) and the *Flag* signal intensity in the TL and IC fractions were quantitated using Adobe Photoshop and normalized to actin signal intensity. IC intensity was calculated as a percentage of TL intensity and S abundance determined by subtraction of the latter from 100%.

4.8. Statistical Analysis

In order to test the primary hypothesis that there are significant differences between the control condition and each of the other conditions (e.g., presence of a variant or expression of beta-subunits), one-way or two-way analysis of variance (ANOVA) was used to conduct all analyses comparing control condition to each of the condition types individually with a Holm-Sidak correction, as appropriate (SigmaPlot® software). Results are presented as mean ± standard error (SEMs). Significance level $p < 0.05$ was considered significant.

Supplementary Materials: Supplementary materials can be found at http://www.mdpi.com/1422-0067/21/14/5057/s1, Figure S1: Effect of $Na_v1.5$ R878C and G1743R variants on I_{Na}, Figure S2: Recovery from inactivation of $K_v4.3$ in presence of SCN5A variants was not affected, Figure S3: Effect of $Na_v1.5$ variants on $K_v4.3$-long, Figure S4: Raw traces of $Na_v1.5$ WT + Na_v 1 +$K_v4.3$-WT or variants, Figure S5: I_{Na} recovery from inactivation was not affected by $K_v4.3$ variants, Figure S6: Separating I_{to} from I_{Na} recordings to assess a potential overlap between the two currents, Figure S7: Raw traces of $Na_v1.5$ + $K_v4.3$ in presence of -subunits, Figure S8: Co-IP full Blot, Figure S9: Cell surface biotinylation full blots.

Author Contributions: conceptualization, J.C.; methodology, J.C.; validation, J.C., N.N., R.C., J.H.; formal analysis, J.C., R.C., J.H.; investigation, J.C., N.N., R.C., C.S.; resources, P.G. and C.A.; data curation, J.C.; writing—original draft preparation, J.C.; writing—review and editing, J.C., P.G., N.N. and C.A.; visualization, J.C.; supervision, J.C., P.G., C.A.; funding acquisition, J.C., P.G., C.A. All authors have read and agreed to the published version of the manuscript.

Funding: This work was supported by a *doctoral grant* provided by the "*CORDDIM*" from the Region Ile de France (2009–2012) to J. Clatot (PI), NIH grants HL47678, HL138103 and HL152201 to C. Antzelevitch (C.A.), W.W. Smith Foundation Grant (C.A.) and the Wistar and Martha Morris Fund (C.A.).

Acknowledgments: We would like thank Alfred George, Jr. for the gift of the HEK293 $Na_v1.1$, $Na_v\beta1$, $Na_v\beta2$ stable cell line.

Conflicts of Interest: The authors declare no conflict of interest.

Abbreviations

AP	Action Potential
BrS	Brugada syndrome
Na_v	Sodium voltage-gated channels
I_{Na}	Inward sodium current
WT	Wild type
ER	Endoplasmic reticulum
$I_{to} = I_A$	Transient outward potassium current
SCA19/22	Spinocerebellar Ataxia type 19 and 22
LOF	Loss of function
GOF	Gain of function

References

1. Antzelevitch, C.; Yan, G.-X.; Ackerman, M.J.; Borggrefe, M.; Corrado, D.; Guo, J.; Gussak, I.; Hasdemir, C.; Horie, M.; Huikuri, H.; et al. J-Wave syndromes expert consensus conference report: Emerging concepts and gaps in knowledge. *J. Arrhythmia* **2016**, *32*, 315–339. [CrossRef] [PubMed]
2. Clatot, J.; Ziyadeh-Isleem, A.; Maugenre, S.; Denjoy, I.; Liu, H.; Dilanian, G.; Hatem, S.N.; Deschênes, I.; Coulombe, A.; Guicheney, P.; et al. Dominant-negative effect of SCN5A N-terminal mutations through the interaction of Nav1.5 α-subunits. *Cardiovasc. Res.* **2012**, *96*, 53–63. [CrossRef] [PubMed]
3. Giudicessi, J.R.; Ye, D.; Tester, D.J.; Crotti, L.; Mugione, A.; Nesterenko, V.V.; Albertson, R.M.; Antzelevitch, C.; Schwartz, P.J.; Ackerman, M.J. Transient outward current (Ito) gain-of-function mutations in the KCND3-encoded Kv4.3 potassium channel and Brugada syndrome. *Heart Rhythm* **2011**, *8*, 1024–1032. [CrossRef]
4. Portero, V.; Wilders, R.; Casini, S.; Charpentier, F.; Verkerk, A.O.; Remme, C.A. KV4.3 Expression Modulates NaV1.5 Sodium Current. *Front. Physiol.* **2018**, *9*, 178. [CrossRef] [PubMed]

5. Duarri, A.; Nibbeling, E.; Fokkens, M.R.; Meijer, M.; Boddeke, E.; Lagrange, E.; Stevanin, G.; Brice, A.; Durr, A.; Verbeek, D.S. The L450F [Corrected] mutation in KCND3 brings spinocerebellar ataxia and Brugada syndrome closer together. *Neurogenetics* **2013**, *14*, 257–258. [CrossRef]
6. Grant, A.O.; Carboni, M.P.; Neplioueva, V.; Starmer, C.F.; Memmi, M.; Napolitano, C.; Priori, S. Long QT syndrome, Brugada syndrome, and conduction system disease are linked to a single sodium channel mutation. *J. Clin. Invest.* **2002**, *110*, 1201–1209. [CrossRef]
7. Lee, Y.-C.; Durr, A.; Majczenko, K.; Huang, Y.-H.; Liu, Y.-C.; Lien, C.-C.; Tsai, P.-C.; Ichikawa, Y.; Goto, J.; Monin, M.-L.; et al. Mutations in *KCND3* cause spinocerebellar ataxia type 22. *Ann. Neurol.* **2012**, *72*, 859–869. [CrossRef]
8. Valdivia, C. A trafficking defective, Brugada syndrome-causing SCN5A mutation rescued by drugs. *Cardiovasc. Res.* **2004**, *62*, 53–62. [CrossRef]
9. Zhang, Y.; Wang, T.; Ma, A.; Zhou, X.; Gui, J.; Wan, H.; Shi, R.; Huang, C.; Grace, A.A.; Huang, C.L.-H.; et al. Correlations between clinical and physiological consequences of the novel mutation R878C in a highly conserved pore residue in the cardiac Na+ channel. *Acta Physiol.* **2008**, *194*, 311–323. [CrossRef]
10. Clatot, J.; Zheng, Y.; Girardeau, A.; Liu, H.; Laurita, K.R.; Marionneau, C.; Deschênes, I. Mutant voltage-gated Na^+ channels can exert a dominant negative effect through coupled gating. *Am. J. Physiol. Heart Circ. Physiol.* **2018**, *315*, H1250–H1257. [CrossRef] [PubMed]
11. Clatot, J.; Hoshi, M.; Wan, X.; Liu, H.; Jain, A.; Shinlapawittayatorn, K.; Marionneau, C.; Ficker, E.; Ha, T.; Deschênes, I. Voltage-gated sodium channels assemble and gate as dimers. *Nat. Commun.* **2017**, *8*, 2077. [CrossRef]
12. Antzelevitch, C.; Patocskai, B. Brugada Syndrome: Clinical, Genetic, Molecular, Cellular, and Ionic Aspects. *Curr. Probl. Cardiol.* **2016**, *41*, 7–57. [CrossRef] [PubMed]
13. Antzelevitch, C.; Yan, G.-X. J-wave syndromes: Brugada and early repolarization syndromes. *Heart Rhythm* **2015**, *12*, 1852–1866. [CrossRef] [PubMed]
14. Di Diego, J.M.; Antzelevitch, C. J wave syndromes as a cause of malignant cardiac arrhythmias. *Pacing Clin. Electrophysiol. Pace* **2018**, *41*, 684–699. [CrossRef] [PubMed]
15. Haïssaguerre, M.; Derval, N.; Sacher, F.; Jesel, L.; Deisenhofer, I.; de Roy, L.; Pasquié, J.-L.; Nogami, A.; Babuty, D.; Yli-Mayry, S.; et al. Sudden cardiac arrest associated with early repolarization. *N. Engl. J. Med.* **2008**, *358*, 2016–2023. [CrossRef] [PubMed]
16. Nof, E.; Vysochek, L.; Meisel, E.; Burashnikov, E.; Antzelevitch, C.; Clatot, J.; Beinart, R.; Luria, D.; Glikson, M.; Oz, S. Mutations in NaV1.5 Reveal Calcium-Calmodulin Regulation of Sodium Channel. *Front. Physiol.* **2019**, *10*, 700. [CrossRef] [PubMed]
17. Matamoros, M.; Pérez-Hernández, M.; Guerrero-Serna, G.; Amorós, I.; Barana, A.; Núñez, M.; Ponce-Balbuena, D.; Sacristán, S.; Gómez, R.; Tamargo, J.; et al. Nav1.5 N-terminal domain binding to α1-syntrophin increases membrane density of human Kir2.1, Kir2.2 and Nav1.5 channels. *Cardiovasc. Res.* **2016**, *110*, 279–290. [CrossRef]
18. Ponce-Balbuena, D.; Guerrero-Serna, G.; Valdivia, C.R.; Caballero, R.; Diez-Guerra, F.J.; Jiménez-Vázquez, E.N.; Ramírez, R.J.; Monteiro da Rocha, A.; Herron, T.J.; Campbell, K.F.; et al. Cardiac Kir2.1 and Nav 1.5 Channels Traffic Together to the Sarcolemma to Control Excitability. *Circ. Res.* **2018**, *122*, 1501–1516. [CrossRef]
19. Keller, D.; Rougier, J.; Kucera, J.; Benammar, N.; Fressart, V.; Guicheney, P.; Madle, A.; Fromer, M.; Schlapfer, J.; Abriel, H. Brugada syndrome and fever: Genetic and molecular characterization of patients carrying mutations. *Cardiovasc. Res.* **2005**, *67*, 510–519. [CrossRef]
20. Eijkelkamp, N.; Linley, J.E.; Baker, M.D.; Minett, M.S.; Cregg, R.; Werdehausen, R.; Rugiero, F.; Wood, J.N. Neurological perspectives on voltage-gated sodium channels. *Brain* **2012**, *135*, 2585–2612. [CrossRef]
21. Zhao, X.-J.; Zhu, C.; Tian, L.-Y.; Fu, Y.-C.; Zhang, Y.; Chen, X.; Huang, Y.; Li, Y. Kv4.3 Modulates the Distribution of hERG. *Sci. Rep.* **2017**, *7*, 17757. [CrossRef]
22. Biliczki, P.; Girmatsion, Z.; Brandes, R.P.; Harenkamp, S.; Pitard, B.; Charpentier, F.; Hébert, T.E.; Hohnloser, S.H.; Baró, I.; Nattel, S.; et al. Trafficking-deficient long QT syndrome mutation KCNQ1-T587M confers severe clinical phenotype by impairment of KCNH2 membrane localization: Evidence for clinically significant IKr-IKs α-subunit interaction. *Heart Rhythm* **2009**, *6*, 1792–1801. [CrossRef] [PubMed]

23. Belau, F.; Metzner, K.; Christ, T.; Ravens, U.; Schaefer, M.; Künzel, S.; Li, W.; Wettwer, E.; Dobrev, D.; El-Armouche, A.; et al. DPP10 is a new regulator of Nav1.5 channels in human heart. *Int. J. Cardiol.* **2019**, *284*, 68–73. [CrossRef] [PubMed]
24. Di Diego, J.M.; Sun, Z.Q.; Antzelevitch, C. I(to) and action potential notch are smaller in left vs. right canine ventricular epicardium. *Am. J. Physiol. Heart Circ. Physiol.* **1996**, *271*, H548–H561. [CrossRef] [PubMed]
25. Calloe, K.; Aistrup, G.L.; Di Diego, J.M.; Goodrow, R.J.; Treat, J.A.; Cordeiro, J.M. Interventricular differences in sodium current and its potential role in Brugada syndrome. *Physiol. Rep.* **2018**, *6*, e13787. [CrossRef] [PubMed]
26. Park, D.S.; Cerrone, M.; Morley, G.; Vasquez, C.; Fowler, S.; Liu, N.; Bernstein, S.A.; Liu, F.-Y.; Zhang, J.; Rogers, C.S.; et al. Genetically engineered SCN5A mutant pig hearts exhibit conduction defects and arrhythmias. *J. Clin. Investig.* **2015**, *125*, 403–412. [CrossRef] [PubMed]
27. Szél, T.; Antzelevitch, C. Abnormal repolarization as the basis for late potentials and fractionated electrograms recorded from epicardium in experimental models of Brugada syndrome. *J. Am. Coll. Cardiol.* **2014**, *63*, 2037–2045. [CrossRef]
28. Patocskai, B.; Antzelevitch, C. Novel Therapeutic Strategies for the Management of Ventricular Arrhythmias Associated with the Brugada Syndrome. *Expert Opin. Orphan Drugs* **2015**, *3*, 633–651. [CrossRef]
29. Durr, A. Autosomal dominant cerebellar ataxias: Polyglutamine expansions and beyond. *Lancet Neurol.* **2010**, *9*, 885–894. [CrossRef]
30. Sharkey, L.M.; Cheng, X.; Drews, V.; Buchner, D.A.; Jones, J.M.; Justice, M.J.; Waxman, S.G.; Dib-Hajj, S.D.; Meisler, M.H. The ataxia3 Mutation in the N-Terminal Cytoplasmic Domain of Sodium Channel Nav1.6 Disrupts Intracellular Trafficking. *J. Neurosci.* **2009**, *29*, 2733–2741. [CrossRef]
31. Sailer, A.; Houlden, H. Recent Advances in the Genetics of Cerebellar Ataxias. *Curr. Neurol. Neurosci. Rep.* **2012**, *12*, 227–236. [CrossRef] [PubMed]
32. Duarri, A.; Jezierska, J.; Fokkens, M.; Meijer, M.; Schelhaas, H.J.; den Dunnen, W.F.A.; van Dijk, F.; Verschuuren-Bemelmans, C.; Hageman, G.; van de Vlies, P.; et al. Mutations in potassium channel kcnd3 cause spinocerebellar ataxia type 19. *Ann. Neurol.* **2012**, *72*, 870–880. [CrossRef] [PubMed]
33. Kurihara, M.; Ishiura, H.; Sasaki, T.; Otsuka, J.; Hayashi, T.; Terao, Y.; Matsukawa, T.; Mitsui, J.; Kaneko, J.; Nishiyama, K.; et al. Novel De Novo KCND3 Mutation in a Japanese Patient with Intellectual Disability, Cerebellar Ataxia, Myoclonus, and Dystonia. *Cerebellum* **2018**, *17*, 237–242. [CrossRef]
34. Nibbeling, E.A.R.; Duarri, A.; Verschuuren-Bemelmans, C.C.; Fokkens, M.R.; Karjalainen, J.M.; Smeets, C.J.L.M.; de Boer-Bergsma, J.J.; van der Vries, G.; Dooijes, D.; Bampi, G.B.; et al. Exome sequencing and network analysis identifies shared mechanisms underlying spinocerebellar ataxia. *Brain* **2017**, *140*, 2860–2878. [CrossRef] [PubMed]
35. Smets, K.; Duarri, A.; Deconinck, T.; Ceulemans, B.; van de Warrenburg, B.P.; Züchner, S.; Gonzalez, M.A.; Schüle, R.; Synofzik, M.; Van der Aa, N.; et al. First de novo KCND3 mutation causes severe Kv4.3 channel dysfunction leading to early onset cerebellar ataxia, intellectual disability, oral apraxia and epilepsy. *BMC Med. Genet.* **2015**, *16*, 1–7. [CrossRef]
36. Coutelier, M.; Coarelli, G.; Monin, M.-L.; Konop, J.; Davoine, C.-S.; Tesson, C.; Valter, R.; Anheim, M.; Behin, A.; Castelnovo, G.; et al. A panel study on patients with dominant cerebellar ataxia highlights the frequency of channelopathies. *Brain* **2017**, *140*, 1579–1594. [CrossRef]
37. You, T.; Mao, W.; Cai, B.; Li, F.; Xu, H. Two novel Brugada syndrome-associated mutations increase KV4.3 membrane expression and function. *Int. J. Mol. Med.* **2015**, *36*, 309–315. [CrossRef]
38. Choi, K.-D.; Kim, J.-S.; Kim, H.-J.; Jung, I.; Jeong, S.-H.; Lee, S.-H.; Kim, D.U.; Kim, S.-H.; Choi, S.Y.; Shin, J.-H.; et al. Genetic Variants Associated with Episodic Ataxia in Korea. *Sci. Rep.* **2017**, *7*, 13855. [CrossRef]
39. Chauveau, S.; Janin, A.; Till, M.; Morel, E.; Chevalier, P.; Millat, G. Early repolarization syndrome caused by de novo duplication of KCND3 detected by next-generation sequencing. *Heartrhythm Case Rep.* **2017**, *3*, 574–578. [CrossRef]
40. Takayama, K.; Ohno, S.; Ding, W.-G.; Ashihara, T.; Fukumoto, D.; Wada, Y.; Makiyama, T.; Kise, H.; Hoshiai, M.; Matsuura, H.; et al. A de novo gain-of-function KCND3 mutation in early repolarization syndrome. *Heart Rhythm* **2019**, *16*, 1698–1706. [CrossRef]
41. Olesen, M.S.; Refsgaard, L.; Holst, A.G.; Larsen, A.P.; Grubb, S.; Haunsø, S.; Svendsen, J.H.; Olesen, S.-P.; Schmitt, N.; Calloe, K. A novel KCND3 gain-of-function mutation associated with early-onset of persistent lone atrial fibrillation. *Cardiovasc. Res.* **2013**, *98*, 488–495. [CrossRef] [PubMed]

42. Petitprez, S.; Zmoos, A.-F.; Ogrodnik, J.; Balse, E.; Raad, N.; El-Haou, S.; Albesa, M.; Bittihn, P.; Luther, S.; Lehnart, S.E.; et al. SAP97 and Dystrophin Macromolecular Complexes Determine Two Pools of Cardiac Sodium Channels Na_v 1.5 in Cardiomyocytes. *Circ. Res.* **2011**, *108*, 294–304. [CrossRef] [PubMed]
43. Shy, D.; Gillet, L.; Abriel, H. Targeting the Sodium Channel Na_V 1.5 to Specific Membrane Compartments of Cardiac Cells: Not a Simple Task! *Circ. Res.* **2014**, *115*, 901–903. [CrossRef]
44. Rougier, J.-S.; Essers, M.C.; Gillet, L.; Guichard, S.; Sonntag, S.; Shmerling, D.; Abriel, H. A Distinct Pool of Nav1.5 Channels at the Lateral Membrane of Murine Ventricular Cardiomyocytes. *Front. Physiol.* **2019**, *10*, 834. [CrossRef] [PubMed]